

## ANTI-LAMBDA/ANTI-PROTON RATIOS AT THE AGS\*

G. J. Wang, R. Bellwied, C. Pruneau, and G. Welke*Department of Physics and Astronomy,**Wayne State University, Detroit, MI 48202, U.S.A.**E-mail: welke@physics.wayne.edu*

We attempt to explain the large  $\bar{\Lambda}/\bar{p}$  ratios measured in heavy ion collisions at 12 A · GeV/c beam momentum within an hadronic framework. The ratios are large compared to corresponding ratios in  $pp$  collisions, and to thermal fits. We show using a simple model and a detailed cascade calculation that different annihilation cross-sections of  $\bar{\Lambda}$ 's and  $\bar{p}$ 's, and the net conversion of  $\bar{p}$ 's to  $\bar{\Lambda}$ 's, do not account for the enhancement. Uncertainties in elementary cross-sections and formation times are also considered.

## I. INTRODUCTION

Anti-Lambda ( $\bar{\Lambda}$ ) cross-sections in heavy ion collisions are of interest because strangeness production is a potential signal for QGP formation. [1–3] The ratio  $\bar{\Lambda}/\bar{p}$  is of special interest since it reflects the production of  $\bar{s}$ -quarks relative to non-strange light anti-quarks, and should increase substantially relative to the production expected from a superposition of  $NN$  collisions, if a QGP is formed.

Recent experiments have reported [4–7] measurements of  $\bar{p}$  and  $\bar{\Lambda}$  production in various heavy ion systems at the Brookhaven AGS and at the CERN SPS. Experiment E859 reports the ratio of  $\bar{\Lambda}$  and  $\bar{p}$  rapidity distributions to be  $3 \pm 1 \pm 1$  in central Si+Pb collisions. [4] This ratio is corrected for finite experiment acceptance, efficiencies, and for  $\bar{p}$  creation from  $\bar{\Lambda}$  decay (feed-down). It also takes into account that neutral  $\bar{\Sigma}$  particles cannot be distinguished from the  $\bar{\Lambda}$  sample. Experiment E864 has measured [5] the  $\bar{p}$  production cross-section in Au+Pb at 11.6 A · GeV/c. They compare this measurement with a similar one from the E878 collaboration that was obtained with a focusing spectrometer, and interpret the difference between the two measurements as an indicator of  $\bar{\Lambda}$  production. E864 estimates that  $\bar{\Lambda}/\bar{p} > 2.3$  at the 98%CI, with a most probable value of 3.5. At the SPS, NA35 has published [6,7]  $\bar{\Lambda}/\bar{p}$  ratios for  $pp$ ,  $pA$ , S+S, S+Ag, and S+Au collisions at 200 A · GeV/c, and they observe a significant rise from 0.25 for  $pp$ -collisions to 1.5 for the heavy ion systems.

It is tempting to interpret the large reported ratios as evidence for the formation of a QGP: Many authors [8–10] have argued that the CERN multi-strange baryon ratios [11–13] can only be described by a QGP scenario. This conclusion is, however, challenged by E864 Au+Au RQMD simulations that find that the  $\bar{p}$  production cross-section appears to be lower than expected from the scaled  $NN$   $\bar{p}$  cross-section.

Here, we shall try to address quantitatively all possible hadronic contributions to the  $\bar{\Lambda}/\bar{p}$  ratio. We restrict calculations to AGS energies and show that “differential annihilation” of the two species and  $\bar{p}$ -to- $\bar{\Lambda}$  conversion processes can indeed enhance the  $\bar{\Lambda}/\bar{p}$  ratio, but we conclude that the effect is not large enough – thus hinting at a production mechanism outside of the standard hadronic interactions. We present these arguments as follows: The observed  $\bar{\Lambda}/\bar{p}$  ratios cannot be explained by a thermal model, unless severe inconsistencies with other measured data, such as the charged pion and kaon cross-sections, are introduced. This has been shown by many authors, [14–16] and we give our own calculation in the next Section. Thermal equilibration is unlikely at present energies, so we consider transport simulations in the rest of the paper, first discussing the relevant cross-sections, then the results for a simple geometrical model, and finally the results of a detailed cascade calculation. Actual measurements of the  $\bar{\Lambda}$  and  $\bar{p}$  cross-sections [17,18] are used, not event generator parametrizations. We shall consider uncertainties in these calculations, particularly those arising from the relatively poorly known  $\bar{\Lambda}$  annihilation, and from particle formation times. Speculative conclusions based on the quantitative discrepancy between calculations and the actual measurements are presented in the last Section.

---

\*Submitted to *Proceedings of the 14th Winter Workshop on Nuclear Dynamics*, Snowbird, Utah, 31 January – 6 February 1998, “Advances in Nuclear Dynamics 4,” W. Bauer and H.G. Ritter, eds. (Plenum Publishing, 1998).

## II. THERMAL MODEL

In a thermal model, the final relative abundance of a particle is determined by both the primary number of this species at freeze-out, and by feed-down from heavier species after freeze-out. We report here results for central Au+Au collisions at 11.6 GeV/ $c$ , and include all mesons with rest mass  $\leq 1$  GeV/ $c^2$ , and all baryons with rest mass  $\leq 1.7$  GeV/ $c^2$ .

We assume thermal and chemical equilibration for freeze-out, so that all relative abundances can be obtained from four parameters: the freeze-out temperature  $T_0$ , the electric chemical potential  $\mu_e$ , the baryonic chemical potential  $\mu_b$ , and the strange chemical potential  $\mu_s$ . Here,

$$\mu_i = q_i \mu_e + b_i \mu_b + S_i \mu_s \quad (2.1)$$

are particle chemical potentials, where  $q_i$ ,  $b_i$  and  $S_i$  are the charge, baryon number and strangeness of species  $i$ , respectively. The thermal fit parameters are obtained by applying the conditions  $|Q/B - 0.40| < 1\%$  and  $|S| < 2\%$ , together with the constraints listed in Table 1. We purposefully choose rather large ranges in these latter constraints to show how difficult it would be to obtain the experimental  $\bar{\Lambda}/\bar{p}$  ratio.<sup>1</sup>

In Table 1, the “errors” on the best fit values for  $T_0$  and the chemical potentials are ranges that lead to results consistent with the constraint intervals.<sup>2</sup> We see that  $\bar{\Lambda}/\bar{p} \lesssim 1.9$ , at best. It is instructive to consider the results graphically. Figure 1(a) shows  $\bar{\Lambda}/\bar{p}$  as a function of  $K^+/K^-$  for various freeze-out temperatures  $T_0$ . Large  $\bar{\Lambda}/\bar{p} > 2$  result only if the freeze-out temperature and/or observed  $K^+/K^-$  ratio are pushed unreasonably high. A similar conclusion follows from Figure 1(b), which shows  $\bar{\Lambda}/\bar{p}$  as a function of  $K^+/\pi^+$ , with  $T_0 = 120 \pm 14$  MeV.

We conclude that the experimental ratio  $\bar{\Lambda}/\bar{p}$  ratio has, at the very least, a significant non-thermal component: the lower experimental bound for the ratio reported by E864 is larger than any reasonable thermal fit would allow.

TABLE 1 Thermal vs experimental particle ratios for central Au+Au collisions at 11.6 GeV/ $c$ . The parameter ranges are  $T_0 = 120 \pm 14$  MeV,  $\mu_b = 556 \pm 19$  MeV,  $\mu_s = 111 \pm 14$  MeV, and  $\mu_e = -14 \pm 2$  MeV.

Ratio	Constraint	Thermal Model	Data		
			Ratio	Rapidity	Ref.
$K^+/\pi^+$	0.16–0.28	$0.23 \pm 0.03$	$0.22 \pm 0.01$	0.5–1.3	[19]
$K^+/K^-$	4.0–6.0	$4.73 \pm 0.53$	$5.0 \pm 1.0$	0.5–1.3	[19]
$K^-/\pi^-$	–	$(3.50 \pm 0.62) \times 10^{-2}$	0.028	1.2–2.0	[20]
$\pi^+/p$	0.6–1.2	$0.71 \pm 0.09$	–	–	–
$\pi^-/p$	0.8–1.4	$1.00 \pm 0.10$	1.00	1.2–2.0	[20]
$\Lambda/p$	–	$0.16 \pm 0.02$	–	–	–
$\bar{p}/p$	–	$(3.48 \pm 3.44) \times 10^{-4}$	–	–	–
$\bar{\Lambda}/\bar{p}$	–	$1.58 \pm 0.30$	–	–	–

## III. CROSS-SECTIONS

Generally, a thermal description is useful for a given particle species if its mean free path is small compared to the system size. This fact alone means that other approaches should also be investigated. We do so in the next two sections, and discuss here the most important physical input, *viz.*, the relevant cross-sections. The following are the relevant processes we shall consider: Firstly, the production of  $\bar{p}$ 's and  $\bar{\Lambda}$ 's:

$$b_1 + b_2 \rightarrow N_1 + N_2 + B + \bar{B} (+\pi) \quad (3.1)$$

$$M + b \rightarrow N + B + \bar{B} (+\pi) \quad (3.2)$$

$$M + M \rightarrow B + \bar{B} (+\pi) \quad (3.3)$$

$$S^+ + S^- \rightarrow B + \bar{B} (+\pi) \quad (3.4)$$

$$(3.5)$$

<sup>1</sup>Our number of  $\bar{\Lambda}$ 's throughout includes  $\bar{\Sigma}^0$ 's, as experiment does not distinguish between the two species.

<sup>2</sup>We note that these parameters are not inconsistent with overall energy conservation considerations. Recall also that  $m_t$  spectra are blue shifted by the presence of strong flow.

$$b + S^+ \rightarrow b + \bar{B} + N (+K^+ + \pi) \quad (3.6)$$

$$M + S^+ \rightarrow N + \bar{B} (+S^+ + \pi) \quad (3.7)$$

Here,  $b$  represents a non-strange baryon,  $N$  a nucleon,  $B$  any baryon,  $M$  a light unflavored meson, and  $S^\pm$  a  $\pm 1$ -strangeness meson. Secondly, (same notation):

$$\bar{p} + b \rightarrow X \quad (3.8)$$

$$b + \bar{\Lambda} \rightarrow S^+ + \pi \quad (3.9)$$

$$S^+ + \bar{b} \rightarrow \bar{\Lambda} + \pi \quad (3.10)$$

$$M + \bar{p} \rightarrow \bar{\Lambda} + \pi + S^- \quad (3.11)$$

$$M + \bar{\Lambda} \rightarrow \bar{b} + S^+ (+\pi) \quad (3.12)$$

We refer to (3.8) and (3.9) as annihilation processes, and (3.10)–(3.12) as conversion processes.

The experimental  $p\bar{p}$  annihilation cross-section is well known, and can be parameterized as

$$\sigma_{p\bar{p}}^{annih}(p_{lab}) = 67 p_{lab}^{-0.7} \text{ mb} , \quad (3.13)$$

where  $p_{lab}$  is the momentum of the “beam” particle in GeV/ $c$  with the “target” at rest. The solid line in Figure 2 shows this parameterization of the data (diamonds). The  $\bar{\Lambda}$  annihilation cross-section, on the other hand, is relatively poorly known, especially in the energy range we are interested in. We model it by assuming that the elastic cross-sections for  $p\bar{\Lambda}$  and  $p\Lambda$  are equal, and then use the data of Ref. [18] to obtain:

$$\sigma_{p\bar{\Lambda}}^{annih}(p_{lab}) = 15 (p_{lab}/10)^{-\alpha} \text{ mb} , \quad (3.14)$$

where the same comments apply as for Eq. (3.13). While the data is best fit by  $\alpha = 0.5$ , the uncertainty is rather large (see Figure 2; the stars are data from Ref. [18]). In fact, one might well argue that the data is consistent with

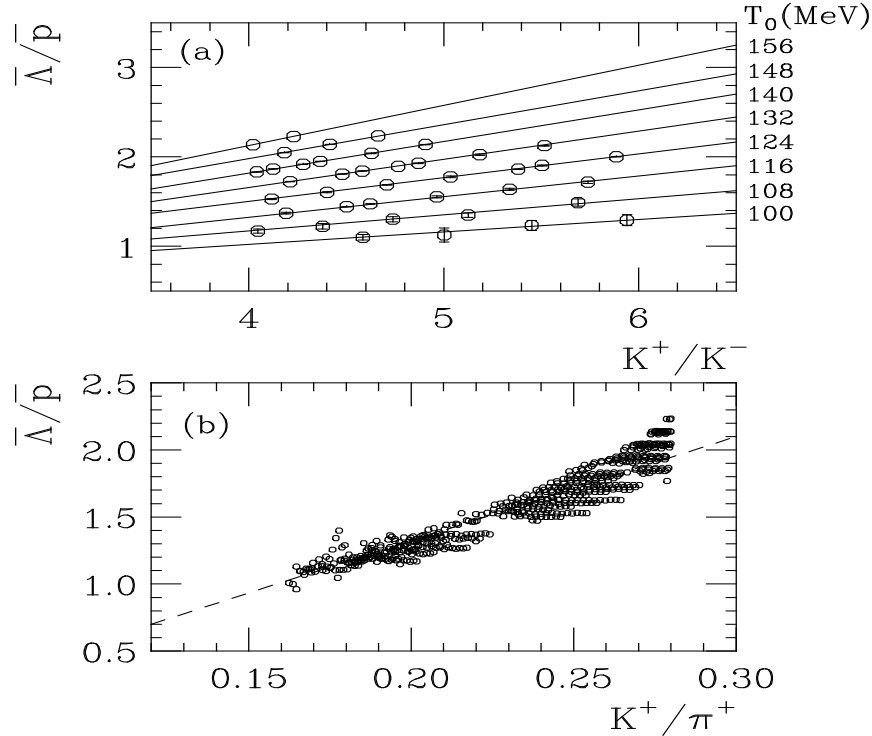


FIG. 1. (a) Thermal  $\bar{\Lambda}/\bar{p}$  ratios as a function of  $K^+/K^-$  for various freeze-out temperatures  $T_0$ . (b) Thermal  $\bar{\Lambda}/\bar{p}$  ratios as a function of  $K^+/\pi^+$ , with  $T_0 = 120 \pm 14$  MeV. Error bars and scatter points indicate values consistent with constraints not shown; the lines are to guide the eye only.

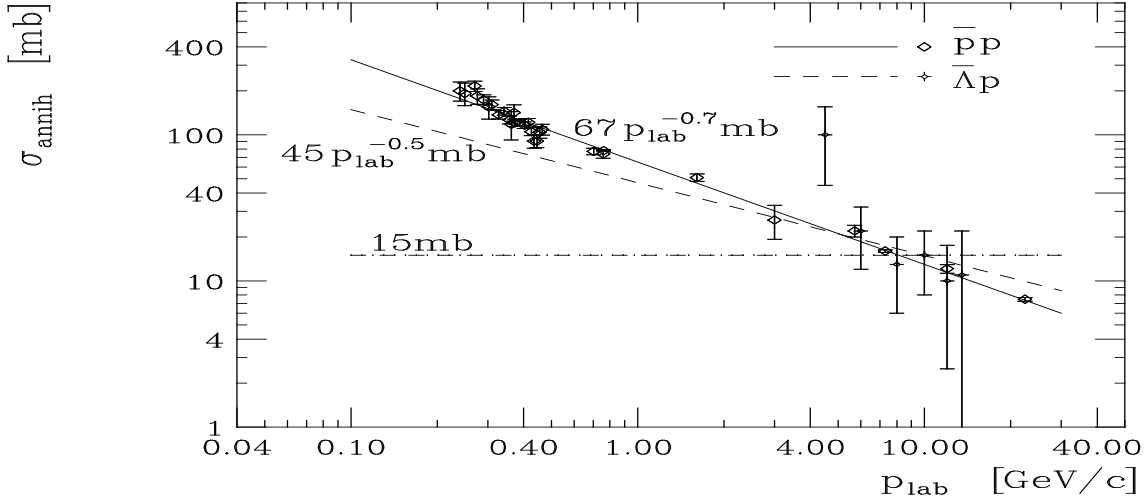


FIG. 2. The annihilation cross-sections of  $\bar{p}$  ( $\bar{\Lambda}$ ) with nucleons, as a function of the incident momentum of the  $\bar{p}$  ( $\bar{\Lambda}$ ).

$\alpha = 0.3$  For  $\alpha = 0.7$  the  $\bar{\Lambda}$  data is practically indistinguishable from the  $\bar{p}$  data. We shall subsequently investigate the behavior of  $\bar{\Lambda}/\bar{p}$  with  $\alpha$ .

The  $\bar{p}$  and  $\bar{\Lambda}$  scattering with mesons is also an important process we need to consider. Broadly speaking, we have three types of collision: (1) thermalization of  $\bar{p}$ 's and  $\bar{\Lambda}$ 's through elastic collisions; (2) production of resonances that eventually decay back into  $\bar{p}$ 's or  $\bar{\Lambda}$ 's; and (3), most importantly, net conversion of  $\bar{p}$ 's to  $\bar{\Lambda}$ 's. Chief amongst these is

$$\bar{p} + K^+ \rightarrow \bar{\Lambda} \quad (\text{or resonances of } \bar{\Lambda}) \quad , \quad (3.15)$$

for which we know the charge conjugate reaction to have a sizeable cross-section. The process (3.15) thus contributes significantly to reducing the  $\bar{p}$  abundance while enhancing the  $\bar{\Lambda}$  abundance in the final state. Given the pronounced strangeness enhancement in large systems such as Au+Au, the process (3.15) should be a relatively important piece of the  $\bar{\Lambda}/\bar{p}$  “puzzle.”

Finally, we shall need the  $\bar{\Lambda}/\bar{p}$  ratio in  $pp$  collisions. At  $\sqrt{s} \sim 20$  GeV, it has a value [21–24] of 0.25–0.30. At AGS energies ( $\sqrt{s} \sim 5$  GeV) its value is less established. Using Refs. [21–23], we infer a value of  $\sim 0.2$ , but we shall use a value of 0.25 throughout this work. This implies that the heavy ion  $\bar{\Lambda}/\bar{p}$  ratios we obtain in subsequent calculations will be upper bounds.

#### IV. GEOMETRIC MODEL CALCULATION

It is often rather useful to have a simple understanding of cascade output. We shall perform such a detailed cascade simulation in the next Section; here we model  $\bar{p}$  and  $\bar{\Lambda}$  production, annihilation and net conversion ( $\bar{p}$ ,  $\bar{n}$  to  $\bar{\Lambda}$ ,  $\bar{\Sigma}$ ) in a simple geometric model. Our starting point are the rate equations

$$\begin{aligned} dN_{\bar{p}} &= -\left(\frac{1}{\lambda_a} + \frac{1}{\lambda_c}\right) N_{\bar{p}} dz \\ dN_{\bar{\Lambda}} &= -\frac{1}{\Lambda_a} N_{\bar{\Lambda}} dz + \frac{1}{\lambda_c} N_{\bar{p}} dz \quad , \end{aligned} \quad (4.1)$$

where  $\lambda_a$  and  $\lambda_c$  are the annihilation and net conversion mean free paths for  $\bar{p}$ 's, respectively, and  $\Lambda_a$  is the annihilation mean free path for the  $\bar{\Lambda}$ . We take the initial  $\bar{\Lambda}/\bar{p}$  ratio from  $pp$  collisions:

<sup>3</sup>QCD sum rules imply a behavior consistent with  $\alpha \sim 0$ .

$$\left(\frac{N_{\bar{\Lambda}}}{N_{\bar{p}}}\right)^{AA}\Big|_{z=0} \equiv \frac{N_0^{\bar{p}}}{N_0^{\bar{\Lambda}}} = \left(\frac{N_{\bar{\Lambda}}}{N_{\bar{p}}}\right)^{pp} \lesssim 0.25 ,$$

as discussed in the previous section. The final number of  $\bar{p}$ 's or  $\bar{\Lambda}$ 's depends on the distribution of the length  $z$  of nuclear matter that the anti-particle passes through:

$$N = \langle N(z) \rangle .$$

Integrating Eqs. (4.1) gives the number of  $\bar{p}$  and  $\bar{\Lambda}$  after they have passed through a fixed length  $z$  of nuclear matter:

$$N_{\bar{p}}(z) = N_0^{\bar{p}} e^{-(1/\lambda_a + 1/\lambda_c)z} \quad (4.2)$$

$$N_{\bar{\Lambda}}(z) = N_0^{\bar{\Lambda}} e^{-z/\Lambda_a} + 2 \frac{N_0^{\bar{p}}}{1 + \frac{\lambda_c}{\lambda_a} - \frac{\lambda_c}{\Lambda_a}} \left( e^{-z/\Lambda_a} - e^{-(1/\lambda_a + 1/\lambda_c)z} \right) . \quad (4.3)$$

The factor of two has been introduced to account for the net conversion of  $\bar{n}$ 's to  $\bar{\Lambda}$ 's.

Next, we need to model the geometry of the collision. We shall assume that  $z$  is related to the combined thickness of the beam and target nuclei  $t$  via

$$z = \beta t ,$$

where  $\beta < 1$  is a constant. It measures the effect of matter expansion, the local average momentum distribution, *etc.* The distribution of  $t$  in a central  $AA$  collision is

$$p(t) = \frac{dt^3}{(4R)^3} , \quad (4.4)$$

where  $R$  is the nuclear radius. This equation allows us to compute the survival probability  $P_s = \langle e^{-z/\lambda} \rangle$  of a  $\bar{p}$  or  $\bar{\Lambda}$  as a function of  $R$ ,  $\lambda$  and  $\beta$ . The analysis for  $AB$  collisions is similar.

It remains to discuss the mean free paths. Generally,

$$\frac{1}{\lambda_j} = \sum_i \int dp_{lab} \rho_i(p_{lab}) \sigma_{ji}(p_{lab}) \frac{dN_j}{dp_{lab}} , \quad (4.5)$$

where  $p_{lab}$  is the momentum of the  $\bar{p}$  or  $\bar{\Lambda}$  measured in the rest frame of the target  $i$  (nucleons, pions or kaons). Also,  $\rho_i$  is the density of target species  $i$ ,  $\sigma_{ji}$  is the corresponding cross-section, and  $dN_j/dp_{lab}$  is the distribution of  $p_{lab}$ . Since the factor  $\beta$  already takes into account any changes in density,  $\rho_i$  should be regarded as the density for which no expansion occurs.

A rough approximation for  $\lambda_a$  follows assuming that the  $\bar{p}$  and  $\bar{\Lambda}$  are produced at rest in the  $NN$  frame, and are annihilated by the nucleons streaming by. In this case,  $p_{lab} \sim \sqrt{s/4 - m_p^2} \sim 2.1$  GeV, with  $\rho \sim 0.16$  fm<sup>-3</sup>, and therefore  $\lambda_a \sim 1.6$  fm.<sup>4</sup> A more detailed calculation that accounts for residual  $\bar{p}$  motion in the  $NN$  frame gives  $\lambda_a \sim 2.0$  fm. Similarly, using appropriate cross-sections and thermal densities, we obtain

$$\begin{aligned} \Lambda_a &\approx 4.2 (3.76)^{-\alpha} \text{ fm} \\ \lambda_c^{(1)} &\approx 180 \text{ fm} \\ \lambda_c^{(2)} &\approx 88 \text{ fm} \\ \lambda_c &\equiv \frac{\lambda_c^{(1)} \lambda_c^{(2)}}{\lambda_c^{(1)} + \lambda_c^{(2)}} \approx 59 \text{ fm} \end{aligned}$$

where  $\lambda_c^{(1)}$  and  $\lambda_c^{(2)}$  are the net conversion mean free paths due to collisions with  $(N, \pi)$  and  $K^+$ , respectively.

The dependence of the two components of the  $\bar{\Lambda}/\bar{p}$  ratio (*viz.*, annihilation and conversion), are shown in Figure 3 for a central, symmetric ( $AA$ ) collision, as a function of the effective size of the system,  $R_{eff} \equiv \beta R$ . The ratio

---

<sup>4</sup>Note that  $z/\lambda$  is Lorentz invariant; we perform calculations in the rest frame of the nucleus.

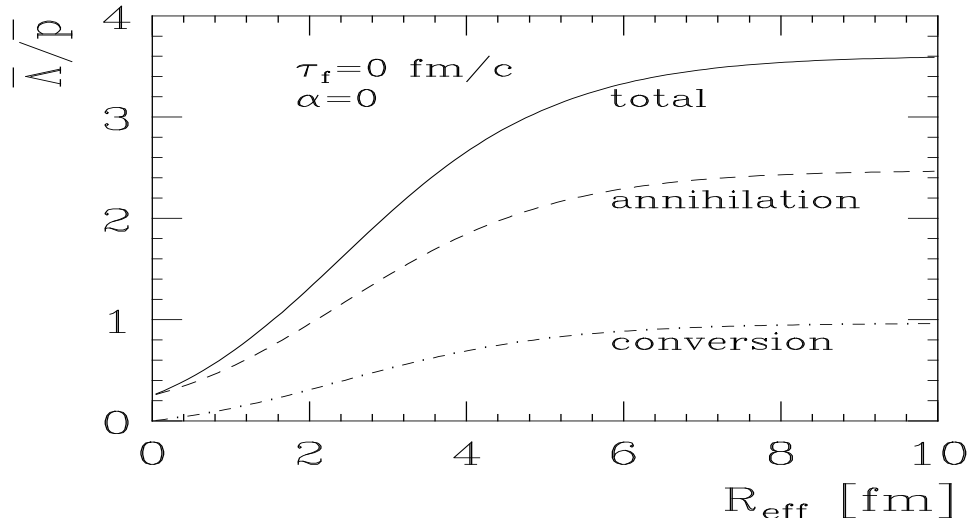


FIG. 3.  $\bar{\Lambda}/\bar{p}$  as a function of  $R_{eff} \equiv \beta R$  for a central AA collision, with  $\alpha = 0$  and zero formation time (solid line). Individual contributions from annihilation and conversion are also shown.

saturates for large  $R_{eff} \gtrsim 6$  fm/c because peripheral collisions play an increasingly important role; the ratio of survival probabilities tends to the ratio of mean free paths cubed. On the other hand, for truly infinite matter all anti-particles pass through a common large length, and  $\bar{\Lambda}/\bar{p}$  is exponentially increasing with  $R_{eff}$ .

The significant discrepancy between the data and our calculation (see also next Section) may indicate that the ratio of core-produced  $\bar{p}$ 's to peripherally produced  $\bar{p}$ 's is larger than predicted by the simple binary hadron-hadron collision scenario.

The solid lines in Figure 4 show the final values of  $\bar{\Lambda}/\bar{p}$  from this simple geometric model, if we use  $\beta = 0.5$ . The agreement with the cascade calculation (circles; see next Section) is very good.

## V. CASCADE CALCULATION

The production rate of  $\bar{p}$ 's or  $\bar{\Lambda}$ 's is only  $O(10^{-2})$  per event at the AGS, and cascade calculations are rather CPU intensive. We shall therefore perform an effective calculation of the survival probability by putting  $\bar{p}$ 's or  $\bar{\Lambda}$ 's in by hand, wherever and whenever a collision occurs in which the energy is sufficient for a  $p\bar{p}$  or  $\Lambda\bar{\Lambda}$  pair to be produced. Thus we assume that the pair production does not depend on energy, once above threshold.<sup>5</sup> The evolution of nucleons, pions and kaons is not allowed to be influenced by the presence of  $\bar{p}$ 's or  $\bar{\Lambda}$ 's – we restore particles that interacted with  $\bar{p}$ 's or  $\bar{\Lambda}$ 's to their pre-collision kinematics.

We may then calculate the  $\bar{\Lambda}/\bar{p}$  ratio via the survival probabilities  $P_s$

$$\frac{\bar{\Lambda}}{\bar{p}} = r_p \frac{P_s(\bar{\Lambda})}{P_s(\bar{p})} + 2r_c \frac{\bar{\Lambda}^c}{\bar{p}^s}, \quad (5.1)$$

where  $\bar{p}^s$  is the number of surviving  $\bar{p}$ 's and  $\bar{\Lambda}^c$  the number of converted  $\bar{\Lambda}$ 's. Also,  $r_p \sim 0.25 \pm 0.1$  is the  $\bar{\Lambda}/\bar{p}$  ratio in  $pp$  collisions, while  $r_c \approx 0.25$  is a correction factor.<sup>6</sup> The factor two accounts for the conversion of  $\bar{n}$ 's to  $\bar{\Lambda}$ 's.

To illustrate the effect of differential annihilation versus net conversion, we show in Table 2 the different components of Eq. (5.1) for different  $\alpha$  and  $\tau = 0$  in central Au+Au collisions at AGS energies. For small  $\alpha$  (small  $\bar{\Lambda}$  annihilation cross-section),  $\bar{\Lambda}/\bar{p}$  enhancement results almost entirely from differential annihilation. As  $\alpha$  increases, the survival probability of a  $\bar{\Lambda}$  and a  $\bar{p}$  become equal, and the sole enhancement in the final ratio results from conversion.

<sup>5</sup>Also, we assume that the production is not medium dependent.

<sup>6</sup>We overestimate  $\bar{\Lambda}$ -production because we assume that all collisions of non-strange anti-baryons with positive strange mesons result in a  $\bar{\Lambda}$ .

TABLE 2 Survival probabilities, the conversion rate, and final  $\bar{\Lambda}/\bar{p}$  ratio for various  $\alpha$  and  $\tau = 0$  fm/c, in a central Au+Au collision.

$\alpha$	$P_s(\bar{\Lambda})$ (%)	$P_s(\bar{p})$ (%)	$\bar{\Lambda}^c/\bar{p}^s$	$\bar{\Lambda}/\bar{p}$
0.0	$12.1 \pm 0.3$	$1.5 \pm 0.1$	$0.75 \pm 0.07$	$2.4 \pm 1.0$
0.2	$6.0 \pm 0.2$	$1.5 \pm 0.1$	$0.45 \pm 0.06$	$1.2 \pm 0.5$
0.4	$3.3 \pm 0.2$	$1.5 \pm 0.1$	$0.38 \pm 0.06$	$0.7 \pm 0.3$
0.7	$1.5 \pm 0.05$	$1.5 \pm 0.1$	$0.16 \pm 0.02$	$0.3 \pm 0.1$

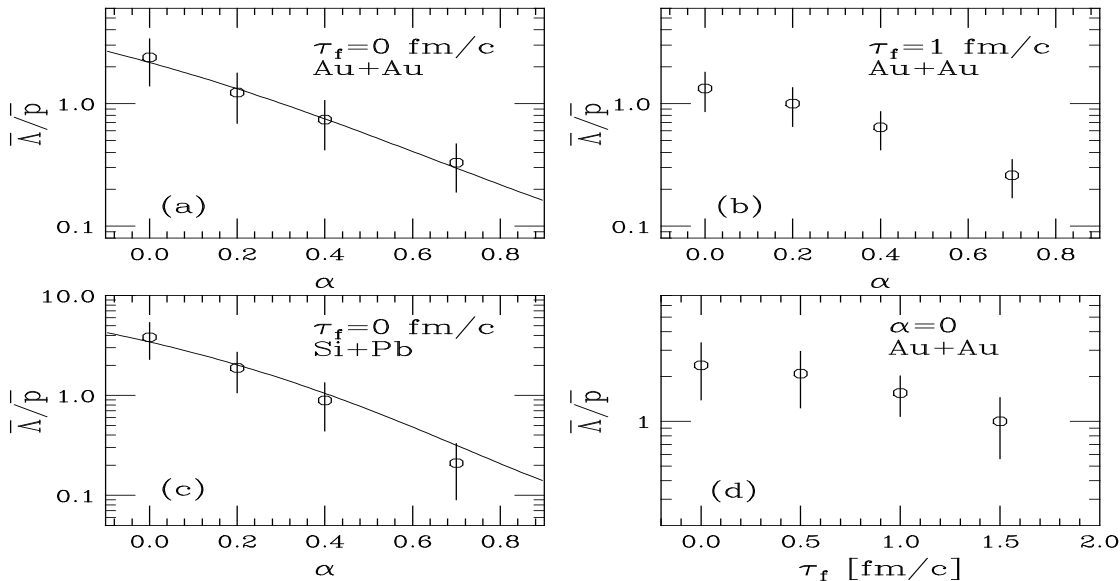


FIG. 4. Cascade  $\bar{\Lambda}/\bar{p}$  ratios for various  $\alpha$ ,  $\tau$  and systems. The solid lines are for the geometric model with  $\beta = 0.5$ .

We show in Figure 4 the final  $\bar{\Lambda}/\bar{p}$  ratios for several values of  $\alpha$  and  $\tau$  for various systems. The solid lines are results from our simple geometric model using  $\beta = 0.5$ , and show that the simple geometrical model predicts the ratios rather well. We note that the ratio is larger in Si+Pb collisions than in Au+Au collisions, both in our calculation and in experiment. Also, note that (1) realistic values for  $\alpha$  are probably closer to 0.5 than 0.0; (2) formation times are probably not zero; and (3) our initial (*i.e.*,  $pp$ )  $\bar{\Lambda}/\bar{p}$  ratio is probably an over-estimate. We thus conclude that in our present calculation  $\bar{\Lambda}/\bar{p} \sim 1$  and most definitely  $\lesssim 2$  for the Au+Au system ( $\lesssim 3$  for Si+Pb).

## VI. CONCLUSIONS

The  $\bar{\Lambda}/\bar{p}$  ratio in  $NN$  collisions at AGS energies is  $\lesssim 0.25$ , heavy ion experiments measure much larger values. The ratio can only be pushed to values above 2 with much difficulty in a hadronic thermal model with chemical equilibration. For Au+Au, using upper limits of  $K^+/\pi^+ = 0.30$ ,  $K^+/K^- = 6.0$ , and  $T_0 = 140$  MeV, we obtain an upper limit of  $\bar{\Lambda}/\bar{p} \sim 2$ , below the E864 98%-lower confidence limit of 2.3.

We have considered a non-equilibrium description, and presented results from a simple geometric model and a detailed cascade calculation. The geometric model does rather well in reproducing trends in the data. Chief inputs to our calculations are the  $\bar{\Lambda}$  and  $\bar{p}$  annihilation cross-sections with nucleons, as well as processes that convert  $\bar{p}$ 's into  $\bar{\Lambda}$ 's. The  $\bar{\Lambda}$  annihilation cross-section is relatively poorly known, but it may be argued that it is somewhat less than  $\bar{p}$  annihilation at AGS energies. Our parameter  $\alpha$  controls this difference, with  $\alpha = 0$  corresponding to the greatest difference, and  $\alpha = 0.7$  corresponding to a cross-section that is practically indistinguishable from  $\bar{p}$  annihilation. Currently, the cross-section data is best fit by  $\alpha = 0.5$ .

In Au+Au cascade simulations at AGS energies, the largest  $\bar{\Lambda}/\bar{p}$  ratio obtainable is  $\sim 3.5$ , for  $\alpha = 0$  and  $\tau = 0$  fm/c. Both these input values are extreme. What we currently believe to be more reasonable inputs lead to a value of  $\bar{\Lambda}/\bar{p} \sim 1$ , far from the lower bound of the E864 experiment.

Interestingly, higher  $\bar{\Lambda}/\bar{p}$  ratios result in central Si+Pb collisions, both in our calculations and in experiment. Within our model this has a simple geometric explanation: For Si+Pb, the  $\bar{p}$ 's and  $\bar{\Lambda}$ 's are produced close to the beam axis, leading to a larger average nuclear thickness that the anti-particle must traverse. We also note that at higher energies the difference between the  $\bar{\Lambda}$  and  $\bar{p}$  annihilation cross-section practically vanishes. One might therefore predict (in hindsight) that  $\bar{\Lambda}/\bar{p}$  at the SPS should be lower than at the AGS, as indeed observed.

We conclude that the large  $\bar{\Lambda}/\bar{p}$  ratios in AGS heavy ion collisions are not easily explained by hadronic mechanisms. QGP formation might be a possible solution, but a more accurate measurement of the  $\bar{\Lambda}$  annihilation cross-section in the relevant energy range is sorely needed before any more definite conclusion can be reached.

This work was supported in part by the U.S. Department of Energy under Grant No. DE-FG02-93ER40713.

## VII. REFERENCES

1. E.V. Shuryak, *Phys. Rep.* 115:151 (1984).
2. P. Koch et al., *Phys Rep.* 142:167 (1986).
3. J. Rafelski, *Phys. Rep.* 88:331 (1982).
4. Y.D. Wu for the E802/E859 Coll.,  $\bar{p}$  and  $\bar{\Lambda}$  production in Si+Au collisions at the AGS, *in*: "Proceedings of Heavy Ion Physics at the AGS: HIPAGS 96," C. Pruneau, G. Welke, R. Bellwied, S. Bennett, J Hall and W Wilson eds., Wayne State University, Detroit (1996), p. 37.
5. J. Lajoie for the E864 Coll., Antiproton production in 11.5 A · GeV/c Au+Pb nucleus collisions, *in*: "HIPAGS 96," *ibid.*, p. 59.
6. D. Röhrich for the NA35 Coll., STRANGENESS 96, Budapest, May 96
7. J. Günther for the NA35 Coll., *Nucl. Phys.* A590:487c (1995).
8. J. Letessier et al., *Phys. Rev.* D51:3408 (1995).
9. J. Letessier, *Nucl. Phys.* A590:613c (1995).
10. J. Sollfrank et al., *Z. Phys.* C61:659 (1994).
11. E. Judd for the NA36 Coll., *Nucl. Phys.* A590:291c (1995).
12. D. Dibari for the WA85 Coll, *Nucl. Phys.* A590:307c (1995).
13. J.B. Kinson for the WA97 Coll., *Nucl. Phys.* A590:317c (1995).
14. P. Braun–Munzinger et al., *Phys. Lett.* B344:43 (1995).
15. P. Braun–Munzinger et al., *Phys. Lett.* B365:1 (1996).
16. E. Schnedermann, and U. Heinz, *Phys. Rev.* C50:1675 (1994).
17. S. Gjesdal et al., *Phys. Lett.* B40:152 (1972).
18. F. Eisele et al., *Phys. Lett.* B60:297 (1976); B60:1067 (1976), and references therein.
19. M. Gonin for the E802 Coll., Meson  $\bar{p}$  production from the E802 and E866 experiments at the AGS, *in*: "Heavy–Ion Physics at the AGS: HIPAGS 93," G. Stephans, S. Steadman, and W. Kehoe eds., MIT Laboratory for Nuclear Science, Cambridge (1993) p. 184 .
20. H. Sako for the E866 Coll., Antiproton production in 11.7 A · GeV/c Au+Au collisions from E866, *in*: "HIPAGS 96," *ibid.*, p. 67.
21. V. Blobel et al., *Nucl. Phys.* B69:454 (1974).
22. M. Antinucci et al., *Lett. Nuovo Cim.* 6:121 (1973).
23. J. Whitmore, *Phys. Rep.* 10:273 (1974).
24. M. Gaździcki, and D. Röhrich, *Z. Phys.* C71:55 (1996).